Chemical Composition and Sulfur Speciation in Bulk Tissue by X-Ray Spectroscopy and X-Ray Microscopy: Corneal Development during Embryogenesis

Elena Koudouna,[†] Giulia Veronesi,[‡] Imran I. Patel,[§] Marine Cotte,[‡] Carlo Knupp,[†] Francis L. Martin,[§] and Andrew J. Quantock[†]*

[†]Structural Biophysics Group, School of Optometry and Vision Sciences, Cardiff University, Wales, United Kingdom; [‡]X-ray Microscopy Beamline ID21, European Synchrotron Radiation Facility, Grenoble cedex, France; and [§]Centre for Biophotonics, Lancaster Environment Centre, Lancaster University, Bailrigg, Lancaster, United Kingdom

ABSTRACT The chemical composition and sulfur (S) speciation of developing chick corneas at embryonic days 12, 14, and 16 were investigated using synchrotron scanning x-ray fluorescence microscopy and x-ray absorption near-edge structure spectroscopy. The aim was to develop techniques for the analysis of bulk tissue and identify critical physicochemical variations that correlate with changes in corneal structure-function relationships. Derived data were subjected to principal component analysis and linear discriminant analysis, which highlighted differences in the elemental and S species composition at different stages of embryonic growth. Notably, distinct elemental compositions of chlorine, potassium, calcium, phosphorus, and S altered with development during the transition of the immature opaque cornea to a mature transparent tissue. S structure spectroscopy revealed developmentally regulated alterations in thiols, organic monosulfides, ester sulfate, and inorganic sulfate species. The transient molecular structures and compositional changes reported here provide a deeper understanding of the underlying basis of corneal development during the acquisition of transparency. The experimental and analytical approach is new, to our knowledge, and has wide potential applicability in the life sciences.

INTRODUCTION

Developmentally regulated changes in the biochemical composition of the cornea are believed to underlie the acquisition of transparency (1,2). Pioneering early studies characterized tissue morphogenesis and microanatomical restructuring (3,4), whereas others suggested that pivotal changes in the chemical and physicochemical signatures, particularly of sulfated glycosaminoglycans (GAGs), might underlie the maturation of the corneal extracellular matrix, the establishment of its architecture, and the onset of transparency (5–7). More contemporary studies have sought to characterize the transition of the embryonic cornea from an opaque structure to an optically transparent one using a variety of biochemical, immunochemical, or spectroscopic approaches (8–12). In the main, these have been directed at the sulfation patterns of GAGs in the corneal stroma. Investigators have long used synchrotron radiation to probe the ultrastructure of collagen-rich tissues such as cornea, including that of the developing chick (13,14). Now, advances in x-ray absorption spectroscopy and fluorescence microscopy at synchrotron sources provide noninvasive alternatives to traditional biochemical characterizations of biological tissues. This offers scope to enhance our understanding of molecular changes in intact tissues, and allows for study of altered physiology or pathology, wound healing events or age-related changes. Here, we apply these techniques to the study of the chick cornea during embryonic development at day 12 (Fig. 1 *A*), day 14 (Fig.1 *B*), and day 16 (Fig. 1 *C*).

Synchrotron x-ray microscopy and spectroscopy generate large, complex data sets containing a high number of variables; these require powerful computational data reduction and visualization algorithms to facilitate exploratory analysis. Principal component analysis (PCA) followed by linear discriminant analysis (LDA) is a valuable approach for the interrogation of such complex data (15). PCA and LDA techniques are linear transformations, which transform data to a new coordinate system such that the new set of variables are linear combinations of the original variables. For preliminary data reduction and to further visualize variances of spectra in a select number of principal components, PCA has had widespread usage in the exploration of derived data sets following midinfrared spectroscopy (15–18) and, less commonly, x-ray absorption near-edge structure (XANES) spectroscopy (19,20). The PCA-LDA approach for XANES data analysis is an alternative to standard curve fitting methods, because it allows one to readily handle a much larger data set and, therefore, to increase the statistical significance of the results; moreover, when applied to x-ray fluorescence (XRF) data, it allows insights into differential ionic contents, providing therefore a valuable semiquantitative standard-free alternative to the more commonly employed standard-based fully quantitative methods, when relative changes in concentrations are sought. In this study, we set out to establish XRF and XANES spectroscopy as

Submitted January 17, 2012, and accepted for publication May 2, 2012.

*Correspondence: quantockaj@cardiff.ac.uk

Editor: James Grotberg.

0006-3495/12/07/0357/8 $2.00

doi: 10.1016/j.bpj.2012.05.036

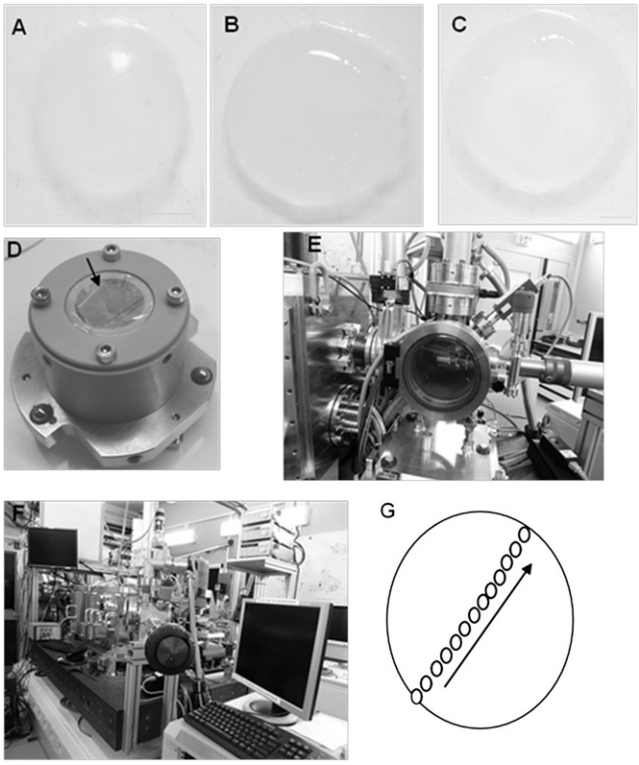

FIGURE 1 Sample preparation for acquisition of XRF and XANES spectra. (*A*) Dissected chick cornea at embryonic day 12, (*B*) day 14, and (*C*) day 16. (*D*) The sample is sandwiched between two sheets of ultralene foil and mounted on the sample holder. The arrow indicates the surface that will be exposed to the x-ray beam. (*E*) The Simulatore di Ambiente Spaziale (SAS) vacuum chamber for sample mounting. Once the sample is placed inside the SAS is pumped. When high vacuum is reached the sample can be introduced into the scanning x-ray microscope by means of a transfer cane. (*F*) Photograph of the scanning x-ray microscope at the end station ID 21, ESRF. Scale bar equals to 1 mm. (*G*) Diagram indicating from where the S speciation XANES point spectra for every developing chick cornea were obtained. For each sample spot, five XANES spectra were acquired. Black arrow shows the direction at which ~13 points were selected to be analyzed.

technologies to interrogate intact biological tissue, with subsequent application of PCA-LDA to investigate the changing chemical environment in corneal development during embryogenesis.

MATERIALS AND METHODS

Sample preparation

Fertilized chicken eggs were obtained from a commercial hatchery (Henry Stewart & Co., Louth, Lincolnshire, UK) and incubated at 37.5°C in a humidified chamber (Brinsea Products, Sandford, UK). At embryonic days 12, 14, and 16 of incubation, as validated by Hamilton-Hamburger staging (21,22), corneas were carefully dissected at their edge using surgical tools. All animal work was carried out in accordance with the Association for Research in Vision and Ophthalmology statement for the use of animals for ophthalmic and vision research and in agreement with local ethical rules.

Synchrotron XRF microscopy

For XRF microscopy studies, four corneas per embryonic day were sandwiched between parafilm-covered glass slides and allowed to dry overnight at room temperature. Data were collected at the endstation ID 21 of the European Synchrotron Radiation Facility (ESRF, Grenoble, France) using a scanning x-ray microscope working in the energy range 2–9.2 keV and optimized for x-ray microfluorescence and microspectroscopy imaging of elemental distributions (23). The samples were held between Ultralene foil (SPEX-CERTIPREP), mounted in air at room temperature on the sample holder (Fig.1 *D*, Fig. 1 *E*), and then introduced to the x-ray microscope and measured at high vacuum. Five regions per cornea per embryonic day were selected from the central region of the cornea and an XRF spectrum with an integration time of 60 s was acquired at each location. The incoming photon energy was tuned at 4.1 keV to excite the core electrons of elements up to Ca, with a flux of 3.6×10^9 photons/s. A beam size of 100 μm was obtained using a pinhole. The emitted fluorescence signals were measured with an energy dispersive silicon drift diode detector (XFlash 5100 from Bruker, Germany). The elemental composition of the developing corneas was obtained by extracting the XRF spectra using PyMCA software (24). Thanks to the detecting geometry and operation under vacuum, the background contribution to the XRF spectra was very low, thus background subtraction was not necessary before PCA analysis (see Supporting Material Fig. S1). The distance between the silicon drift diode detector and the sample, and the size of the beam (and therefore the photon flux at sample) were kept constant throughout the experiments to assure the comparability of spectra. Data analysis was restricted to the range 1.0–4.3 keV and was performed using OPUS 5.5 software (Bruker Optics).

Synchrotron x-ray microspectroscopy

S XANES spectroscopy experiments were performed with the scanning x-ray microscope (Fig.1 *F*) at beamline ID 21 at the ESRF to interrogate developmental changes in sulfur speciation. The instrumentation used was the same as described for XRF. Three corneas at embryonic days 12 and 14, and four at embryonic day 16 were flattened and sandwiched between ultralene foil-covered glass slides. To minimize degradation, the corneas were placed onto dry ice and transferred to −80°C storage until the synchrotron x-ray microspectroscopy experiments could be conducted. Approximately 1 h prior the experiment, slow nitrogen flow was used to defrost the corneas and avoid oxidation events. The samples were then mounted in air at room temperature on the sample holder before being measured at high vacuum. Thirteen locations were interrogated across the diameter of the cornea (Fig.1 *G*). The S speciation of the selected areas was assessed by acquiring five spectra per spot. The x-ray energy was tuned from 2.46 to 2.53 keV with a flux of 5.4×10^9 photons/s, a step size of 0.25eV, and an integration time per energy point of 0.1 s. This resulted in a total integration time of 0.5 s per point over the five spectra. The XANES spectrum was extracted using PyMCA, and a linear background extrapolated from a linear fit of the pre-edge region was subtracted using OPUS (Bruker Optics). XANES spectra were normalized by setting the edge jump to 1 in MATLAB (The MathWorks, Natick, MA).

Computational analysis

Multivariate analysis was performed on the XRF and XANES spectra using MATLAB R2009b software with an in-house graphical user toolkit for spectroscopy (25). PCA and LDA were applied to the data. PCA was used for preliminary data reduction and visualization of variance between each cornea in an unsupervised manner. LDA, a supervised method, was then applied to allow visualization of the maximum variance between the different developmental corneas. Scores plots, loadings, and cluster vector plots were derived to interpret the results of multivariate analysis.

RESULTS

XRF spectra of the developing chick cornea

Four isolated chick corneas at days 12, 14, and 16 of development were analyzed using the scanning x-ray microscope at the ID 21 beamline of the ESRF. For every corneal sample, 20 independent spectral acquisitions were obtained, derived from five randomly selected areas. PyMCA software (24) was used to extract all the spectra, and identification of the different elements present in the corneal sample was assessed by comparison with tabulated energy values for XRF emission lines (Fig. 2 and Table S1).

Observable differences were apparent in the average spectral ranges, 2000–2300 eV and 2620–3311 eV (Fig. S1). To further extract the major discriminating elemental composition responsible for between-category variation (corneas from a particular day formed one category), multivariate computational analysis with PCA (Fig. S2) followed by LDA (Fig. 3 *A*) was employed in the photon energy region range 1000–4300 eV. In this analysis, chick corneas at days 12, 14, and 16 were discovered to be segregated along the 1st linear discriminant (LD1) factor. Corneas at developmental day 16 vs. days 12 and 14 were shown to be distinct, whereas no clear difference in LD1 was seen between day 12 and day 14. The 2nd linear discriminant (LD2) factor discriminated day 14 from days 12 and 16. No distinction in LD2 was found between day 12 and day 16. PCA-LDA clustering indicated a degree of within-category heterogeneity in the corneas at developmental days 12 and 14, whereas data for the day 16 corneas was more homogeneous. Exploiting the derived loadings plot (Fig. 3 *B*), it is possible to identify the major elemental groupings responsible for distinguishing the average spectrum of each category (i.e., each developmental day) from the average spectra of the other categories. Along LD1, the main distinctive elements responsible for the compositional segregation of chick corneas at day 16 compared to earlier developmental days, listed in order of importance, are phosphorus (P; 2012 eV), sulfur (S; 2306 eV), chlorine (Cl; 2620 eV), and calcium (Ca; 3688 eV). Along LD2, the major elements responsible for discrimination of corneas at day 14 compared to days 12 and 16 are Cl, P, potassium (K; 3312 eV), and Ca. The generation of a cluster vectors plot of the data, which is a linear combination of the PCA-LDA loadings, was obtained from the center of the PCA-LDA scores cluster (Fig. 3 *C*). This allows us to obtain differences from multiple loadings in a single plot, rather than along a single axis (e.g., LD1 or LD2) (15). This analysis indicates that P followed by S and Cl are the main elements that contribute to the

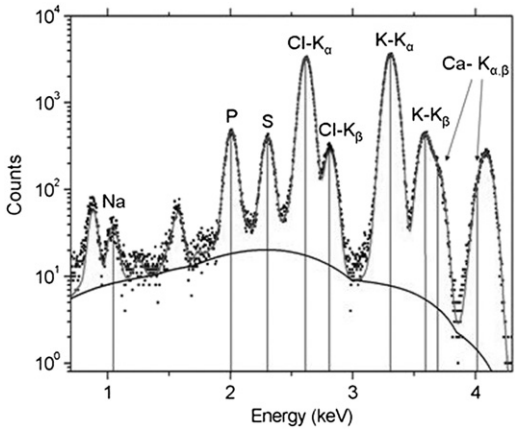

FIGURE 2 XRF spectrum fitted with PyMCA. Experimental XRF spectrum (*dots*) acquired on a 100 μm- diameter region of cornea at embryonic day 14, and its best fitting curve (*upper solid line*) calculated with PyMCA; the background is indicated by the lower solid line. The emission energies relative to the main elemental species encountered in the specimen are reported on the graph, labeled with the corresponding elemental symbol.

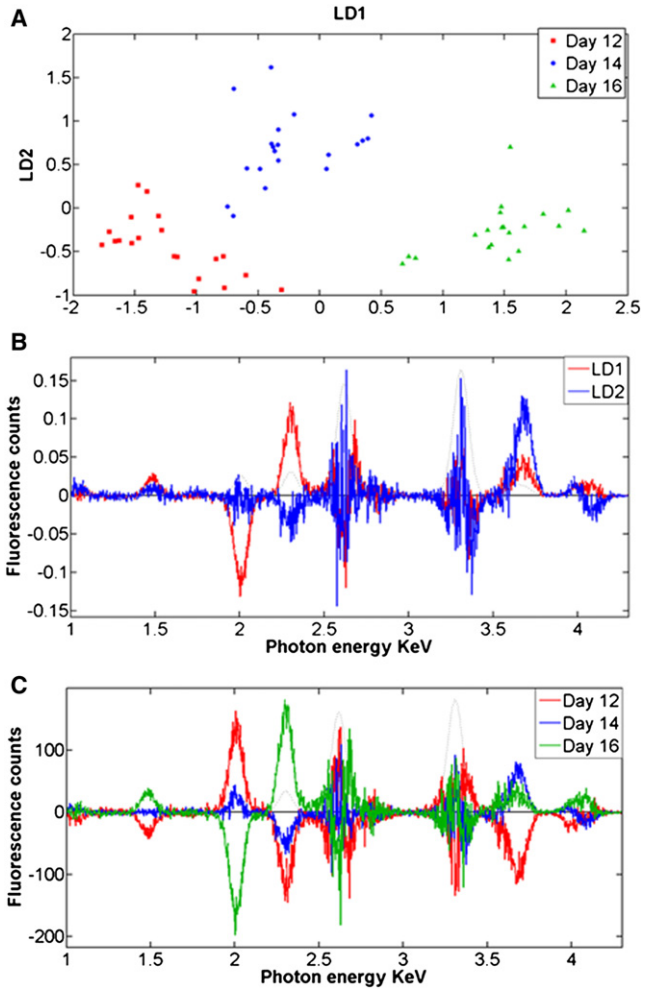

FIGURE 3 Identification of chemical composition alterations of developing chick corneas using PCA-LDA computation of XRF spectra. (*A*) Two-D PCA-LDA scores plot of chick corneas at different developmental days: day 12 (*red squares*) vs. day 14 (*blue circles*) vs. day 16 (*green triangles*). (*B*) PCA-LDA loadings plot of developmental chick corneas at day 12, day 14, and day 16 with linear discriminant components (LDs) as follows: LD1 (*red*) and LD2 (*blue*). (*C*) Corresponding PCA-LDA cluster vectors plot of developmental chick corneas at day 12 vs. day 14 vs. day 16.

biochemical diversity between categories as the chick cornea develops and becomes transparent. K and Ca have little impact on the XRF microscopy differences between corneas at distinct developmental stages.

X-ray absorption near-edge structure spectroscopy of the developing chick cornea

Given the presumed importance of the sulfonation status of corneal GAGs in corneal structural modulation, S K-edge XANES spectroscopy was performed to assess the role of this element's speciation in corneal development. Three corneal samples per embryonic day 12 and 14 along with four corneal samples of embryonic day 16 were interrogated and S XANES point spectra were acquired. The energy position of the peaks in the near-edge region of the absorption coefficient of S alters in the range 2469–2483 eV (26). The assorted S-containing compounds in the corneal samples were evaluated by comparing the absolute energy values to the respective energies for standard sulfur compounds obtained from previous studies as summarized in Table 1. It should be noted that it is not possible to distinguish between inorganic sulfate (SO_4^{2-}) and ester sulfate (R-O-SO_3) because their XANES spectra peak energies are identical (2482.5 ± 0.5 eV), as has been reported in previous studies that investigated the S speciation by XANES microspectroscopy in humic and fulvic acids (27), in marine sediments (28), and in soils and soil particles (26). This is also the case for the differentiation between thiols (R-SH) and organic monosulfides (R-S-R′) because the peak energies of these S-containing compounds are also similar (Table 1) (29). These caveats aside, XANES data can provide important information about the biomolecular status of S in tissues. Our data clearly disclose changes in the character of S during corneal morphogenesis with corresponding average S XANES spectra (Fig. 4) providing information on the major S species, thiols, and organic monosulfides (2.4734 keV), inorganic sulfate, and ester sulfate (2.4835 keV).

A large number of XANES point spectra were acquired to achieve study robustness. Otherwise, it is difficult to distinguish whether similarities or differences in the S species are within-category or between-category. Thus, multivariate analysis was applied to the 2.46–2.49 keV spectral region. PCA was performed to reduce the data and visualize segregation in an unsupervised fashion (Fig. S3), whereas PCA-LDA was applied to extract variance in a supervised manner and highlight between-category differences (Fig. 5 *A*). The analysis reveals distinct clustering and between-category segregation. Specifically, PCA-LDA showed that corneas at days 14 and 16 of development are more homogeneous with respect to their content of S species. In contrast, day 12 corneas exhibited more heterogeneity. Noticeably, some overlap is seen between corneas of developmental days 12 and 14 suggestive of progressive chemical alterations. PCA-LDA loadings plots (Fig. 5 *B*) highlighted the S forms that are responsible for spectral variance and inter-category discrimination. Certainly, LD1 contributes toward segregation of developmental corneas at day 16 vs. days 12 and 14 with contributions mainly associated with inorganic sulfate and ester sulfate (2.483 keV), but also with thiols and organic monosulfides (2.4736 keV). LD2 contributes to day 12 and day 14 segregation, but its spread mainly reflects an intracategory variation at day 12. The data indicate that thiols and organic monosulfides are primary contributors

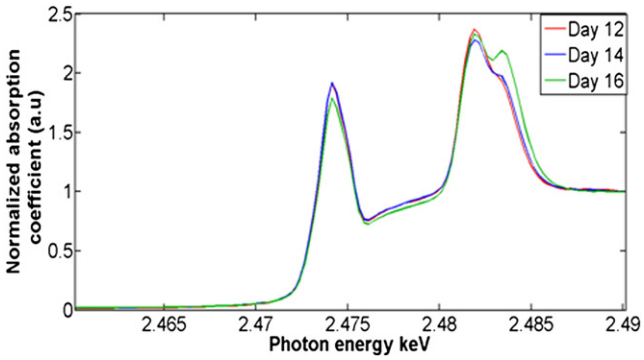

FIGURE 4 S speciation alterations in the developing chick cornea. S K-edge x-ray absorption near-edge spectroscopy means spectra for the embryonic chick corneas at days 12 (*red*), 14 (*blue*), and 16 (*green*) of development.

TABLE 1 Peak energies of the first-order X-ray resonance lines for S species (compilation of literature data)

			Peak energies eV (Reference number)		
S form		Example	(27)	(37)	(38)
Elemental S	S^o		2472.5	2472.5	
Organic polysulfide	R-S-S-S-R′			2473	
Organic disulfide	R-S-S-R′	Cystine	2472.8	2473	2472
Thiols	R-SH	Cysteine		2473.5	2473.5
Organic monosulfides	R-S-R′	Methionine	2473.1	2473.5	2473.5
Sulfoxide	R-S=O	Methionine sulfoxide		2476	2476
Ester sulfate	R-O-SO_3	Chondroitin sulfate	2482.5	2483.5	2482
Inorganic sulfate	SO_4^{2-}	Sodium sulfate	2482.5	2483.5	2483

Peak energies of the first-order x-ray resonance lines for S-containing compounds vary in the range between 2469 and 2483 eV. The absolute peak energy values for distinct sulfur species obtained by other researchers differ slightly from one another.

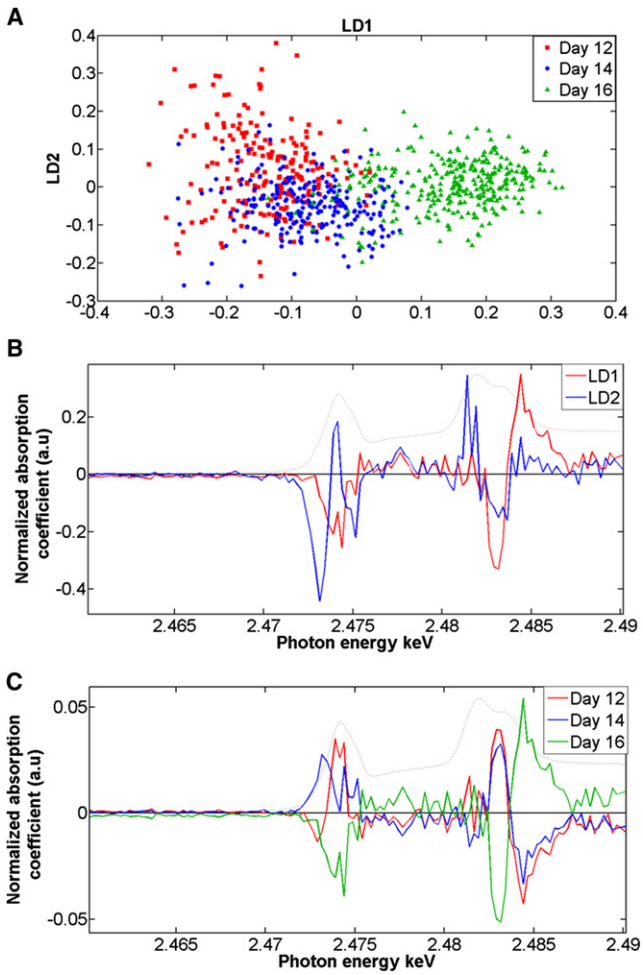

FIGURE 5 Identification of distinct S species alterations in developmental chick corneas using PCA-LDA computation following XANES spectroscopy. (*A*) Two-D PCA-LDA scores plot of chick corneas at different developmental days: day 12 (*red squares*) vs. day 14 (*blue circles*) vs. day 16 (*green triangles*). (*B*) PCA-LDA loadings plot of developing corneas at day 12 vs. day 14 vs. day 16 with LD components as follows: LD1 (*red*) and LD2 (*blue*). (*C*) Corresponding PCA-LDA cluster vectors plot of developmental chick cornea at day 12 vs. day 14 vs. day 16.

for separation followed by inorganic sulfate and ester sulfate. A cluster vectors plot indicated that the influential discriminating sulfur species are thiols and organic monosulfides, organic disulfides (2.4725 keV), inorganic sulfate, and ester sulfate, which all showed remarkable differences among the developmental corneas (Fig. 5 *C*) at days 12, 14, and 16.

Embryonic day 12 vs. embryonic day 14

Further analysis was carried out on chick corneas at embryonic day 12 vs. embryonic day 14 to elucidate the differences and similarities at this developmental period just before the cornea starts to become transparent. PCA-LDA scores plots disclosed a marked overlap in the data sets from day 12 and day 14 corneas (Fig. 6 *A*). The corresponding cluster vectors plot (Fig. 6 *B*) compares day 12 vs. day 14 spectra on the vector plot and vice versa, indicating that the distinguishing species are thiols and organic monosulfides, inorganic sulfate, and ester sulfate.

Embryonic day 12 vs. embryonic day 16

Unlike the day 12 vs. day 14 comparison, further multivariate analysis of data from chick corneas at embryonic day 12 vs. embryonic day 16 showed clear segregation of the two categories. The 1-D PCA-LDA scores plot revealed a relatively small overlap between the two categories (Fig. 6 *C*) reflecting the variance in the S speciation between the two embryonic days. The corresponding cluster vectors plot showed the key distinguishing S species associated with the segregation of the two categories (Fig. 6 *D*), and these, in order of importance are inorganic sulfate and ester sulfate, thiols, and organic monosulfides.

Embryonic day 14 vs. embryonic day 16

Chick corneas at day 14 of development were compared and contrasted to embryonic day 16 corneas and the corresponding PCA-LDA scores plot indicated a clear overlap between the two categories (Fig. 6 *E*). In regard to the cluster vectors plot (Fig. 6 *F*), however, there are major differences in the S speciation between the two developmental time points. The S species that are responsible for the segregation between the two categories are primarily inorganic sulfate and ester sulfate. Minor variance is also observed in the thiols and organic monosulfides species between the two developmental stages.

DISCUSSION

XRF microscopy and XANES spectroscopy with subsequent multivariate analysis (PCA-LDA) were used to provide new, to our knowledge, insights into the biochemical changes of extracellular matrix molecules during tissue morphogenesis in the chick cornea. PCA-LDA scores plots indicated differences between embryonic corneas at days 12, 14, and 16 of development on the basis of the distances between clusters. Loadings plots and cluster vectors plots further identified the chemical entities responsible for segregation of the tissue samples.

Importantly, our results revealed changes in the chemical environment of Cl, K, and Ca elements that contribute to the segregation of data sets at days 12, 14, and 16 of development. These are potentially important ions that will impact on the fixed negative charge density in the corneal extracellular matrix, which itself, is predominantly generated by transient mobile ion binding (30). Developmental alterations in the ionic environment of Cl^{-}, K^{+}, and Ca^{2+} may underlie changes in the physicochemical corneal architecture that help make the tissue transparent to light. The

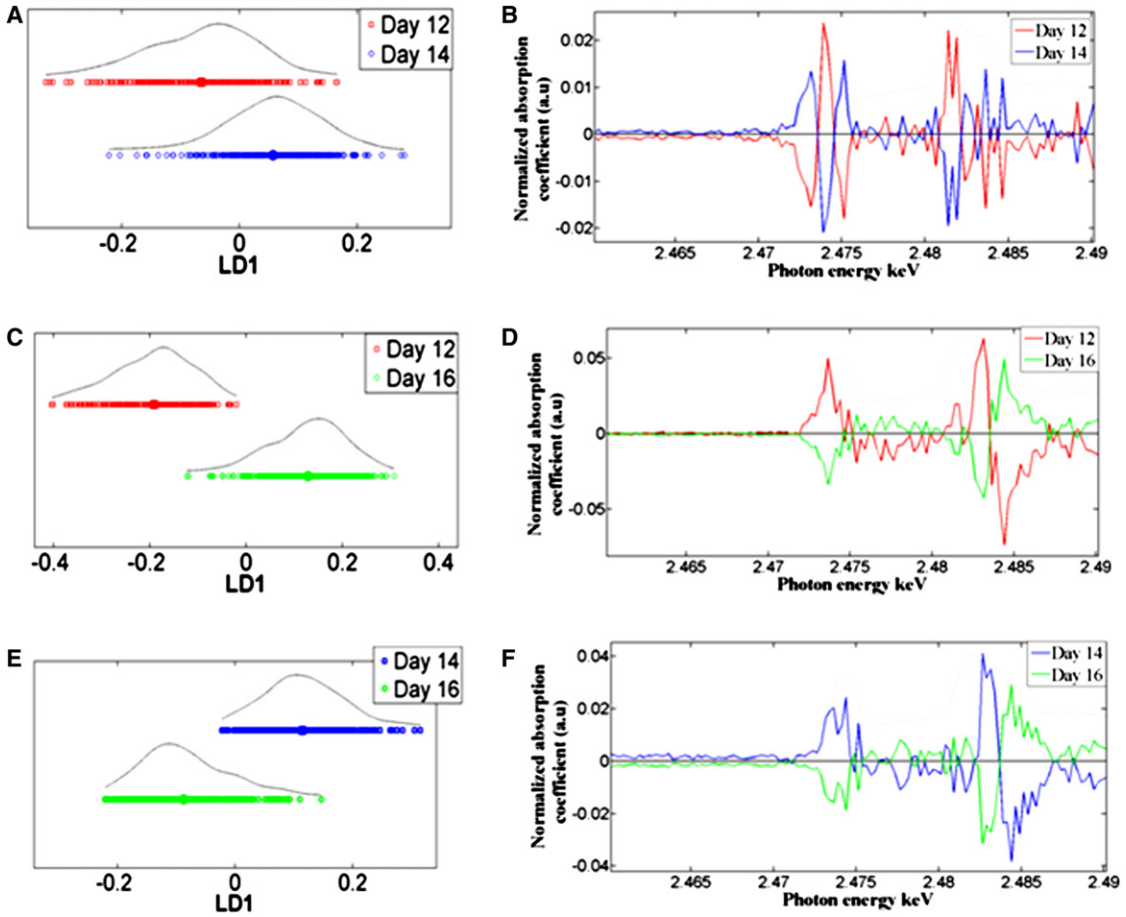

FIGURE 6 PCA-LDA scores and cluster vectors plots of embryonic corneas at days 12, 14, and 16 of development following XANES spectroscopy analysis. (*A*) One-D PCA-LDA scores plot of embryonic day 12 vs. embryonic day 14 and (*B*) the corresponding cluster vectors plot. (*C*) One-D PCA-LDA scores plot of embryonic day 12 vs. embryonic day 16, and (*D*) the corresponding cluster vectors plot. (*E*) One-D PCA-LDA scores plot of embryonic day 14 vs. embryonic day 16, and (*F*) the corresponding cluster vectors plot.

corneal stroma is predominantly composed of collagen fibrils that are uniform in diameter and regularly spaced. This tissue-specific arrangement allows light transmission through the cornea and is based on the interference of light scattered by individual collagen fibrils (31–33). Ion binding within the cornea is believed to be crucial in determining the net surface charge on collagen fibrils, which in turn helps govern the surface-to surface interactions between fibrils, and hence their arrangement (30). This concept is supported by studies of corneas loaded with various concentrations of chloride in which it was shown that chloride ions regulated the fixed negative charge of the corneal matrix and led to a strong dependence on tissue transparency (34). Thus, changes of the chemical environment of Cl may involve binding of chloride ions to collagen fibrils in the corneal stroma, reflecting the changes of the corneal molecular environment and fibrillar architecture. This may well be manifest in the transition of the developing chick corneas from an opaque tissue at days 12 and 14 to a more transparent one at day 16. We also point out that as the charge must be balanced regardless of the involved charge carriers, chloride ions alone are unlikely to be able to influence the tissue charge. There might be an increase in basic residues (amino acids) that lead to an increase in the net positive charge, which in turn must be balanced by chloride ions as negative charge carriers. Similarly, the degree of sulfonation of GAG might affect the concentration of cations such as K+ or Ca^{2+} to balance the negative charge. In this sense, chloride or potassium only reflect the changes in the molecular environment (proteins and glycans) and cannot affect the net charge independently. Correlating the results of the scores, loadings and cluster vector plots it was further discovered that the molecular environment of P changed markedly over the developmental period between embryonic day 12 and day 16. DNA and RNA exhibit numerous phosphate groups, thus, changes in the biochemical character of P are likely related to changes in the presumptive keratocyte population over time and an altered genetic component within these cells.

Sulfated proteoglycans are believed to be key drivers of matrix morphogenesis in developing chick corneas during the acquisition of transparency (5–12). The current study

reports clear changes in the molecular signature of S that occurred between embryonic days 12–16. Subsequent XANES spectroscopy investigation of alterations in the S species present in the developing cornea, followed by PCA-LDA multivariate analysis, highlighted the biochemical molecules that discriminate embryonic corneas at day 12 vs. day 14 vs. day 16. Thiols, organic monosulfides, ester sulfate, and inorganic sulfate were the discriminating variables that underwent a compositional transition during the development of the chick cornea. Variation in the thiol species during embryonic development is likely linked to the N-terminal cysteine consensus sequence region of the small leucine-rich corneal proteoglycans. Developmental differences in the organic monosulfide biochemical peak between days 12–16 are predicted to be associated with protein synthesis and the S methionine amino acid.

Analysis of the XANES spectra suggest that changes in the ester sulfate and inorganic sulfate species that arise during development might be measures of alterations in the keratan sulfate (KS) and chondroitin sulfate/dermatan sulfate (CS/DS) molecular populations. This contention is consistent with studies that report a peak near 2.482 keV, which is attributed to CS (35,36) and document progressive changes in the profiles of KS and CS/DS disaccharides during chick corneal development (9). More specifically, Zhang et al. reported a significant increase in the concentration of sulfated KS around embryonic day 14, in contrast to the concentration of CS/DS disaccharides, which was found to decrease during embryonic development. Mention should also be made of the phenomenon of both low- and high-sulfated KS epitopes existing within individual GAG side chains, and the fact that a differential expression of lesser and highly sulfated KS was evident at developmental days 12 and 15 in experiments conducted using sulfation-specific monoclonal antibodies (12). It is therefore plausible to propose that the changes in the S speciation observed in this study may reflect changes in the degree of sulfonation of low- and high-sulfated GAG side chains. It is instructive to consider the importance of the sulfation pattern of KS for corneal hydration and transparency. In the cornea, the core protein region of a proteoglycan associates with the collagen fibril, whereas the GAG chain extends into the extrafibrillar space. The sulfation status of GAGs is important because it will affect the negative charge of the chains. This, in turn, determines the interactions with other GAGs, the hydrophilic character of the stroma, tissue hydration, and the characteristic fibrillar architecture of the cornea that is necessary for corneal transparency. The current data provide noninvasive evidence, which describe specific changes in the elemental composition of the connective tissue matrix of the embryonic cornea as it develops and becomes transparent, and report how XRF microscopy and XANES spectroscopy can be applied to gain biomolecular information of bulk biological tissue.

SUPPORTING MATERIAL

Supplementary information, three figures, and one table are available at http://www.biophysj.org/biophysj/supplemental/S0006-3495(12)00616-9.

The authors thank Dr. Rob Young and Ms. Frances Jones for help with specimen preparation.

This work was supported by a project grant from the UK Engineering and Physical Sciences Research Council (grant EP/F034970 to AJQ). E.K. is the recipient of a Cardiff University President's Studentship. We thank the European Synchrotron Radiation Facility (ESRF) (http://www.esrf.eu) for providing access to beamtime.

REFERENCES

1. Linsenmayer, T. F., J. M. Fitch, …, D. E. Birk. 1998. Development and roles of collagenous matrices in the embryonic avian cornea. *Prog. Retin. Eye Res.* 17:231–265.
2. Quantock, A. J., and R. D. Young. 2008. Development of the corneal stroma, and the collage-proteoglycan associations that help define its structure and function. *Dev. Dyn.* 237:2607–2621.
3. Coulombre, A. J., and J. L. Coulombre. 1958. Corneal development. I. Corneal transparency. *J. Cell. Physiol.* 51:1–11.
4. Hay, E. D., and J.-P. Revel. 1969. Fine structure of the developing avian cornea. *In* Monographs in Developmental Biology. I. A. Wolsky, N. Y. Tarrytown, and P. S. Chen, editors. S. Karger, Basel, Switzerland, New York. 1–44.
5. Anseth, A. 1961. Glycosaminoglycans in the developing corneal stroma. *Exp. Eye Res.* 1:116–121.
6. Conrad, G. W. 1970. Collagen and mucopolysaccharide biosynthesis in the developing chick cornea. *Dev. Biol.* 21:292–317.
7. Hart, G. W. 1976. Biosynthesis of glycosaminolgycans during corneal development. *J. Biol. Chem.* 251:6513–6521.
8. Cornuet, P. K., T. C. Blochberger, and J. R. Hassell. 1994. Molecular polymorphism of lumican during corneal development. *Invest. Ophthalmol. Vis. Sci.* 35:870–877.
9. Zhang, Y., A. H. Conrad, …, G. W. Conrad. 2005. Detection and quantification of sulfated disaccharides from keratan sulfate and chondroitin/dermatan sulfate during chick corneal development by ESI-MS/MS. *Invest. Ophthalmol. Vis. Sci.* 46:1604–1614.
10. Gealy, E. C., B. C. Kerr, …, J. R. Ralphs. 2007. Differential expression of the keratan sulphate proteoglycan, keratocan, during chick corneal embryogenesis. *Histochem. Cell Biol.* 128:551–555.
11. Young, R. D., E. C. Gealy, …, A. J. Quantock. 2007. Keratan sulfate glycosaminoglycan and the association with collagen fibrils in rudimentary lamellae in the developing avian cornea. *Invest. Ophthalmol. Vis. Sci.* 48:3083–3088.
12. Liles, M., B. P. Palka, …, A. J. Quantock. 2010. Differential relative sulfation of Keratan sulfate glycosaminoglycan in the chick cornea during embryonic development. *Invest. Ophthalmol. Vis. Sci.* 51:1365–1372.
13. Quantock, A. J., S. Kinoshita, …, D. J. Schanzlin. 1998. A synchrotron x-ray diffraction study of developing chick corneas. *Biophys. J.* 74:995–998.
14. Meek, K. M., and A. J. Quantock. 2001. The use of x-ray scattering techniques to determine corneal ultrastructure. *Prog. Retin. Eye Res.* 20:95–137.
15. Martin, F. L., J. G. Kelly, …, M. J. Walsh. 2010. Distinguishing cell types or populations based on the computational analysis of their infrared spectra. *Nat. Protoc.* 5:1748–1760.
16. Kelly, J. G., P. L. Martin-Hirsch, and F. L. Martin. 2009. Discrimination of base differences in oligonucleotides using mid-infrared spectroscopy and multivariate analysis. *Anal. Chem.* 81:5314–5319.

17. Patel, I. I., J. Trevisan, …, F. L. Martin. 2011. Segregation of human prostate tissues classified high-risk (UK) versus low-risk (India) for adenocarcinoma using Fourier-transform infrared or Raman microspectroscopy coupled with discriminant analysis. *Anal. Bioanal. Chem.* 401:969–982.

18. Taylor, S. E., K. T. Cheung, …, F. L. Martin. 2011. Infrared spectroscopy with multivariate analysis to interrogate endometrial tissue: a novel and objective diagnostic approach. *Br. J. Cancer.* 104:790–797.

19. Beauchemin, S., D. Hesterberg, and M. Beauchemin. 2002. Principal component analysis approach for modeling sulfur K-XANES spectra of humic acids. *Soil. Sci. Soc. Am. J.* 66:83–91.

20. Anunziata, O. A., A. R. Beltramone, …, E. Lede. 2011. XANES-PCA analysis of Ti- species in MCM-41 mesoporous silica synthesized by different method. *Appl. Catal. A Gen.* 397:22–26.

21. Hamburger, V., and H. Hamilton. 1951. A series of normal stages in development of the chick embryo. *J. Morphol.* 88:49–92.

22. Hamburger, V. 1992. The stage series of the chick embryo. *Dev. Dyn.* 195:273–275.

23. Barrett, R., B. Kaulich, …, J. Susini. 2000. Current status of the scanning x-ray microscope at the ESRF. *AIP Conf. Proc.* 507:458–463.

24. Solé, A. V., E. Papillon, …, J. Susini. 2007. A multiplatform code for the analysis of energy- dispersive x-ray fluorescence spectra. *Spectrochim. Acta. B.* 62:63–68.

25. Trevisan, J., P. P. Angelov, …, F. L. Martin. 2010. Syrian hamster embryo (SHE) assay (pH 6.7) coupled with infrared spectroscopy and chemometrics towards toxicological assessment. *Analyst (Lond.).* 135:3266–3272.

26. Prietzel, J., J. Thieme, …, I. Kögel-Knabner. 2003. Speciation of sulphur in soils and soil particles by x-ray spectromicroscopy. *Eur. J. Soil Sci.* 54:423–433.

27. Morra, M. J., S. E. Fendorf, and P. D. Brown. 1997. Speciation of sulfur in humic and fulvic acids using x-ray absorption near-edge structure (XANES) spectroscopy. *Geochim. Cosmochim. Acta.* 61:683–688.

28. Vairavamurthy, A., W. Zhou, …, B. Manowitz. 1994. Sulfonates: a novel class of organic sulfur compounds in marine sediments. *Geochim. Cosmochim. Acta.* 58:4681–4687.

29. Xia, K., F. Weesner, …, P. A. Helmke. 1998. XANES studies of oxidation states of sulfur in aquatic and soil humic substances. *Soil. Sci. Soc. Am. J.* 62:1240–1246.

30. Elliott, G. F., and S. A. Hodson. 1998. Cornea, and the swelling of polyelectrolyte gels of biological interest. *Rep. Prog. Phys.* 61:1325–1365.

31. Maurice, D. M. 1957. The structure and transparency of the cornea. *J. Physiol.* 136:263–286.

32. Benedek, G. B. 1971. Theory of transparency of the eye. *Appl. Opt.* 10:459–473.

33. Farrell, R. A., and R. L. McCally. 2000. Corneal transparency. *In* Principles and Practice of Ophthalmology. D. M. Albert and F. A. Jakobiec, editors. WB Saunders, Philadelphia, PA. 629–643.

34. Kostyuk, O., O. Nalovina, …, S. A. Hodson. 2002. Transparency of the bovine corneal stroma at physiological hydration and its dependence on concentration of the ambient anion. *J. Physiol.* 543:633–642.

35. Dauphin, Y., E. J. P. Cuif, …, E. C. T. Williams. 2003. In situ mapping of growth lines in the calcitic prismatic layers of mollusc shells using x-ray absorption near-edge structure (XANES) spectroscopy at the sulphur K-edge. *Mar. Biol.* 142:299–304.

36. Dauphin, Y., J. P. Cuif, …, C. T. Williams. 2006. Microstructure and chemical composition of giant avian eggshells. *Anal. Bioanal. Chem.* 386:1761–1771.

37. Sarret, G., J. Connan, …, L. Eybert-Bèrard. 1999. Chemical forms of sulfur in geological and archaeological asphaltenes from Middle East, France, and Spain determined by sulfur K- and L-edge x-ray absorption near-edge spectroscopy. *Geochim. Cosmochim. Acta.* 63:3767–3779.

38. Vairavamurthy, A., D. Maletic, …, T. Lyons. 1997. Characterization of sulfur-containing functional groups in sedimentary humic substances by x-ray absorption near-edge spectroscopy. *Energy Fuels.* 11:546–553.